Volume 17, Number 4, 2024. pp. 505-516

Jordan Journal of Physics

ARTICLE

On the Optimization of the Transmission Performance of a Broadband A-Sandwich Radome Wall Structure

Manal M. Al-Ali[a], **A. M. Al-Khateeb**[a], **Abd Alghany Jaradat**[a] and **S. H. Mahmood**[b]

[a] *Department of Physics, Yarmouk University, Irbid, Postal Code 21163, Jordan.*
[b] *Department of Physics, The University of Jordan, Amman, Postal Code 11942, Jordan.*

Doi: **https://doi.org/10.47011/17.4.13**
Received on: 23/08/2023; *Accepted on: 28/11/2023*

Abstract: In this work, the microwave propagation characteristics of a planar A-sandwich broadband radome wall structure (Glass epoxy/PU foam/Glass epoxy) were investigated using the characteristic matrix formalism. Theoretical results were compared with those from COMSOL Multiphysics software under varying parameters. At optimal thickness values of the skin (d_1) of the Glass epoxy and the core (d_2) of the PU foam layers, zero reflectance and minimal absorbance (< 2%) were observed at normal incidence, leading to a highly transparent sandwich structure with > 98% transmittance at 3 GHz. Optimization of the core thickness revealed significant improvement in transmittance versus frequency and angle of incidence. The A-sandwich with a skin layer thickness of 0.60 mm and a core layer thickness of 5 mm exhibited high transmittance for a broad frequency band, extending to the X-band at normal incidence. Also, the A-sandwich exhibited high transparency at all angles of incidence for electromagnetic waves with frequencies at the center of the S-band and the X-band. These results demonstrate the feasibility of optimizing planar A-sandwich as a broadband, high-performance radome wall structure for a wide range of frequencies and angles of incidence.

Keywords: A-sandwich radomes, Characteristic matrix, Transmittance, TE and TM waves

1. Introduction

A radar dome (radome) wall constructed from dielectric-dielectric or dielectric-metal combinations is usually used to shield and protect transmitting and receiving antennas and electronic equipment against environmental damage [1–12]. The high performance of the enclosed antenna requires a radome wall with excellent transmission at operating frequencies. Consequently, extensive efforts were devoted to the design of radomes for broadband antenna operation [13–17].

Reflection losses and aberration caused by the radome wall depend on the dielectric constant and the loss tangent of the materials involved in the construction. Therefore, to minimize the impact of the radome on the performance of the antenna, combinations that lead to high absorption should be avoided. In addition, depending on the operational requirements of the antenna, the shape and thickness profile of the radome are also important parameters to meet the structural and environmental requirements [11, 17]. Different structures of the radome wall are usually considered, including thin dielectric walls, half wavelength walls, A-sandwich, B-sandwich, C-sandwich, and multilayered structures [15, 16, 18–20].

Corresponding Author: Manal M. Al-Ali **Email**: manal.alali@yu.edu.jo

The A-sandwich structure, satisfying both the mechanical and electrical requirements, is a practical choice for weather radar radomes [13, 19, 21]. Additionally, A- sandwich designs are used in a wide range of applications [2, 22]. A typical structure consists of two resin glass-fiber skin layers with a dielectric constant near 4 and a loss tangent of0.015, along with a core material, such as honeycomb or foam, with a dielectric constant near 1.15 and a loss tangent of 0.002 [23, 24]. The performance of a high-quality sandwich radome depends on the number of layers, the shape of the radome wall, the thicknesses of skin and core materials, and the overall thickness profile of the structure [1, 2, 5, 6].

The overall reflection, transmission, and absorption response can usually be obtained by adopting the scattering or the propagation matrices, the propagation of the impedances at the interfaces in analogy to transmission lines, or the propagation of the reflection responses [3, 4, 6, 25]. These techniques with forward and backward layer recursions are of most importance for the investigation of wave propagation problems in dielectric thin films, radome wall design, and layered structures. A transfer (transition) matrix relates the electromagnetic fields at two different interfaces (it relates input to output fields), which can be arranged into a scattering matrix that relates the corresponding incoming to outgoing field amplitudes [26–28]. The elements of the scattering matrix (S-parameters) are used widely in the characterization of two- and multi-port networks at microwave frequencies.

In looking for a perfect transmitter with ignorable reflection and absorption responses, we adopt in this article a combination of dielectric materials to construct a planar A-sandwich consisting of a PU Foam dielectric core slab between two identical Glass epoxy skin slabs on either side. The reflection and transmission coefficients are evaluated within the frame of the global characteristic matrix approach [3, 25]. The propagation characteristics of the A-sandwich design with different choices of skin and core layer thicknesses are analyzed, and an optimal sandwich structure is suggested for broadband operation at all angles of incidence.

In this article, theoretical results will be compared with those from COMSOL Multiphysics software. COMSOL Multiphysics is based on the finite element method. It is used to solve and simulate a wide range of physics and engineering problems, in particular, coupled phenomena and multiphysics [29–34]. The effects of skin and core slab thicknesses on the transmission, reflection, and absorption behaviors with the increase of the incident wave frequency and angle of incidence will be investigated by considering representative numerical analysis from theory and simulations. In particular, we are looking for the feasibility of optimizing the A-sandwich radome wall for both TE and TM modes for a broadband high performance at all angles of incidence. The article is organized as follows: In Sec. II we present the geometry and model equations used in characterizing the A-sandwich radome performance. A conventional field-matching technique is used for deriving the global characteristic matrix and the corresponding reflection and transmission coefficients. In Sec. III, we present the transmittance, the reflectance, and the absorbance of electromagnetic waves by the A-sandwich with different layer thicknesses and discuss the dependencies of the performance of the A-sandwich on the frequency and the angle of incidence. Finally, we present the main conclusions of this study in Sec. IV.

2. Model Equations

Figure 1 shows the A-sandwich geometry with free space serving as the input and output media. When the radius of curvature of the radome wall is significantly larger than the wavelength of the incident wave, the radome wall can be treated as a planar multilayer structure with an infinite extent in the *xy*-plane and with finite width in z [6]. We use for the A-sandwich panel two Glass epoxy (G) slabs with $\varepsilon_r = 4$ and a loss tangent $\tan \delta_e = 0.015$, having thicknesses $d_1$and d_3. The core layer consists of PU foam (F), with $\varepsilon_r = 1.15$, $\tan \delta_e = 0.002$, and slab thickness d_2 [23, 24].

The characteristic matrix formalism and its relation to impedance propagation are presented below, along with derivations of expressions for the global reflection ρ and transmission τ coefficients in terms of the elements of the global matrix of a laminated medium [3, 4]. Then we apply the results to analyze the three slabs of the A-sandwich radome wall structure.

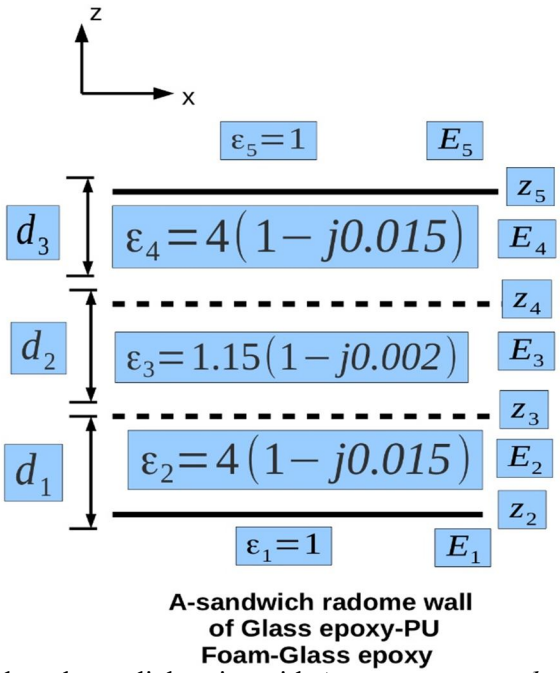

FIG. 1. A-radome wall of three lossy dielectrics with $\Delta z2 = z3 - z2 = d1$, $\Delta z3 = z4 - z3 = d2$, and $\Delta z4 = z5 - z4 = d3$.

Let the plane of incidence be the xz-plane such that $\vec{k}_0 = k_0 \sin\theta_1\, \hat{x} + k_0 \cos\theta_1\, \hat{z}$, where θ_1 stands for the angle of incidence on the first interface. For the transverse electric (TE) mode, the electric field is perpendicular to the plane of incidence such that $\vec{E} = E_y \hat{y}$, whereas the magnetic field is in the plane of incidence such that $\vec{H} = H_x \hat{x} + H_z \hat{z}$.

Considering the y-independent plane wave solution with a typical layer between z_{m-1} and z_m [3], the time-harmonic fields inside the m^{th}-layer of the multilayered structure are given by,

$$E_y = \left(A_m e^{-j\phi_m} + B_m e^{j\phi_m}\right) e^{j(\omega t - k_m x \sin\theta_m)} \quad (1)$$

$$H_x = -\frac{1}{\eta_m}\left(A_m e^{-j\phi_m} - B_m e^{j\phi_m}\right) e^{j(\omega t - k_m x \sin\theta_m)} \quad (2)$$

$$\phi_m = k_m (z - z_m) \cos\theta_m, \quad (3)$$

$$\eta_m = \frac{\omega\mu_m}{k_m} \sec\theta_m\,, k_m^2 = \omega^2 \mu_m \epsilon_m \quad (4)$$

where ω is the frequency of the incident wave, $\mu_m$and $\epsilon_m$are the permeability and permittivity of the m^{th}-layer, respectively, and θ_m is the refraction angle at the m^{th} interface relating the layers m and $m-1$. The continuity of E_y at all interfaces implies $k_m \sin\theta_m = k_0 \sin\theta_1$ for all m-values, namely,

$$\cos\theta_m = \sqrt{1 - \frac{sin^2\theta_1}{\varepsilon_m}}, m = 2, 3, 4. \quad (5)$$

At the interface $z = z_m$, the field components $E_y = E_m$ and $H_x = H_m$ are as follows:

$$E_m = (A_m + B_m) e^{j(\omega t - k_m x \sin\theta_m)}, \quad (6)$$

$$H_m = -\frac{1}{\eta_m}(A_m - B_m) e^{j(\omega t - k_m x \sin\theta_m)}. \quad (7)$$

Similarly, at $z = z_{m-1}$, the field values E_{m-1} and H_{m-1}, are given by

$$E_{m-1} = \left(A_m e^{j\Delta\phi_m} + B_m e^{-j\Delta\phi_m}\right) e^{j(\omega t - k_m x \sin\theta_m)}, \quad (8)$$

$$H_{m-1} = -\frac{1}{\eta_m}\left(A_m e^{j\Delta\phi_m} - B_m e^{-j\Delta\phi_m}\right) e^{j(\omega t - k_m x \sin\theta_m)}, \quad (9)$$

$$\Delta\phi_m = k_m (z_m - z_{m-1}) \cos\theta_m = k_m \Delta z_m \cos\theta_m. \quad (10)$$

Upon solving Eqs. (6) and (7) simultaneously for A_m and B_m in terms of E_m and H_m, we get

$$2A_m = (E_m - \eta_m H_m) e^{-j(\omega t - k_m x)\sin\theta_m}, \quad (11)$$

$$2B_m = (E_m + \eta_m H_m) e^{-j(\omega t - k_m x)\sin\theta_m}, \quad (12)$$

By substituting A_m and B_m into Eqs. (8) and (9), we obtain the following relation between the

input fields (E_{m-1}, H_{m-1}) and the output (E_m, H_m) in matrix form, namely,

$$\begin{pmatrix} E_{m-1} \\ H_{m-1} \end{pmatrix} = \begin{pmatrix} \cos\Delta\phi_m & -j\eta_m \sin\Delta\phi_m \\ -\frac{j}{\eta_m}\sin\Delta\phi_m & \cos\Delta\phi_m \end{pmatrix} \begin{pmatrix} E_m \\ H_m \end{pmatrix}, \quad (13)$$

$$= \begin{pmatrix} k_{m_{11}} & k_{m_{12}} \\ k_{m_{21}} & k_{m_{22}} \end{pmatrix} \begin{pmatrix} E_m \\ H_m \end{pmatrix}, \quad (14)$$

where $k_{m_{ij}}$ stands for the ij^{th} element of the characteristic transmission matrix of the m^{th} layer. Note that E_{m}, H_{m}, $E_{\text{m-1}}$, and $H_{\text{m-1}}$ are the fields on both sides of the m^{th} interface, thus, relating the fields in both layers m and $m-1$. The incident transverse magnetic (TM) mode with $\vec{E}$ being parallel to the plane of incidence can be treated in the same manner without any difficulty. The only change in the above formalism for transverse magnetic waves is to replace the slab intrinsic impedance $\eta_m^{TM} = \frac{\omega\mu_m}{k_m}\sec\theta_m$ by $\eta_m^{TM} = \frac{\omega\mu_m}{k_m}\cos\theta_m$.

A repeated application of the above matrix in a recursive order results in the following relation between the input and the output fields:

$$\begin{pmatrix} E_1 \\ H_1 \end{pmatrix} = \prod_{m=2}^{M} \begin{pmatrix} k_{11} & k_{12} \\ k_{21} & k_{22} \end{pmatrix} \begin{pmatrix} E_M \\ H_M \end{pmatrix}, \quad (15)$$

where $M = 5$ for the A-sandwich under consideration. Note that $M = 2$ and $M = 3$ correspond to a single interface and a slab, respectively. The above product of slab matrices defines the global matrix K of the whole multilayered structure which relates the fields on either side of the structure. Accordingly, we write

$$\begin{pmatrix} E_1 \\ H_1 \end{pmatrix} = \begin{pmatrix} K_{11} & K_{12} \\ K_{21} & K_{22} \end{pmatrix} \begin{pmatrix} E_M \\ H_M \end{pmatrix}, \quad (16)$$

$$E_1 = K_{11}E_M + K_{12}H_M, \quad (17)$$

$$H_1 = K_{21}E_M + K_{22}H_M. \quad (18)$$

In what follows, we express the fields E_1,H_1, E_M, and H_M in terms of the amplitudes of A_1, B_1, A_M, and B_M by using Eqs. (6) and (7). Accordingly, we obtain,

$$A_1 + B_1 = K_{11}(A_M + B_M) + \frac{K_{12}}{\eta_M}(B_M - A_M), \quad (19)$$

$$\frac{B_1 - A_1}{\eta_1} = K_{21}(A_M + B_M) + \frac{K_{22}}{\eta_M}(B_M - A_M), \quad (20)$$

Upon solving Eqs. (19) and (20) simultaneously, we put the result in the following matrix form:

$$\begin{pmatrix} A_1 \\ B_1 \end{pmatrix} = \begin{pmatrix} u_{11} & u_{12} \\ u_{21} & u_{22} \end{pmatrix} \begin{pmatrix} A_M \\ B_M \end{pmatrix}. \quad (21)$$

Here, the elements of the u-matrix are as follows:

$$u_{11} = \frac{1}{2}\left(K_{11} - \frac{1}{\eta_M}K_{12} - \eta_1 K_{21} + \frac{\eta_1}{\eta_M}K_{22}\right) \quad (22)$$

$$u_{12} = \frac{1}{2}\left(K_{11} + \frac{1}{\eta_M}K_{12} - \eta_1 K_{21} - \frac{\eta_1}{\eta_M}K_{22}\right) \quad (23)$$

$$u_{21} = \frac{1}{2}\left(K_{11} - \frac{1}{\eta_M}K_{12} + \eta_1 K_{21} - \frac{\eta_1}{\eta_M}K_{22}\right) \quad (24)$$

$$u_{22} = \frac{1}{2}\left(K_{11} + \frac{1}{\eta_M}K_{12} + \eta_1 K_{21} + \frac{\eta_1}{\eta_M}K_{22}\right) \quad (25)$$

To obtain the microwave propagation characteristics of the A-sandwich of Fig. 1, we assume vacuum as the medium on both sides of the A-sandwich. Applying the above results for five media $M = 5$ with four interfaces, waves will be transmitted in the output medium without any further reflection since the output medium is a free space with an intrinsic impedance $\eta_{M=5} = Z_0$ and extends to infinity. The characteristic matrix K_5 is the unit matrix, therefore, the input as well as the output media will not alter the electromagnetic fields' (E_5 and H_5) transmission through the topmost vacuum layer $M = 5$.

The ratio of the globally transmitted to incident electric field amplitudes defines the global transmission coefficient τ of the A-sandwich structure, which is simply $A_M/A_1 = 1/u_{11}$. On the other hand, using the relation $B_1 = u_{21}A_M = u_{21}\tau A_1$, the ratio of the globally reflected to incident electric field amplitudes $B_1/A_1 = \tau u_{21}$ defines the global reflection coefficient ρ. Accordingly, using Eqs. (22) and (24) we obtain the following relations for these coefficients,

$$\rho = \frac{K_{11} - K_{22} + Z_0 K_{21} - K_{12}/Z_0}{K_{11} + K_{22} - Z_0 K_{21} - K_{12}/Z_0} \quad (26)$$

$$\tau = \frac{2}{K_{11} + K_{22} - Z_0 K_{21} - K_{12}/Z_0} \quad (27)$$

Here, $Z_0 = 377\ \Omega$ is the vacuum impedance and $K_{\alpha\beta}$ is the $\alpha\beta^{th}$-element of the global 2×2-characteristic matrix K of the A-sandwich, namely, $K = K_2K_3K_4$. The matrices K_2 and K_4 are the characteristic matrices of the skin layers, and K_3 is the characteristic matrix of the core layer. For the transverse electric (TE) wave incident at an angle θ_1, the relevant parameters for the analysis of the A-sandwich performance are defined as follows:

$$K_2 = \begin{pmatrix} \cos\Delta\phi_2 & -j\eta_2 \sin\Delta\phi_2 \\ -\frac{j}{\eta_2}\sin\Delta\phi_2 & \cos\Delta\phi_2 \end{pmatrix}, \quad (28)$$

$$K_3 = \begin{pmatrix} \cos\Delta\phi_3 & -j\eta_3 \sin\Delta\phi_3 \\ -\frac{j}{\eta_3}\sin\Delta\phi_3 & \cos\Delta\phi_3 \end{pmatrix}, \quad (29)$$

$$K_4 = \begin{pmatrix} \cos\Delta\phi_4 & -j\eta_4 \sin\Delta\phi_4 \\ -\frac{j}{\eta_4}\sin\Delta\phi_4 & \cos\Delta\phi_4 \end{pmatrix}, \quad (30)$$

$$\Delta\phi_2 = \frac{\omega}{c_0}\sqrt{\varepsilon_2}\,\Delta z_2 \cos\theta_2\,, \eta_2 = \frac{Z_0}{\sqrt{\varepsilon_2}}\sec\theta_2, \quad (31)$$

$$\Delta\phi_3 = \frac{\omega}{c_0}\sqrt{\varepsilon_3}\,\Delta z_3 \cos\theta_3\,, \eta_3 = \frac{Z_0}{\sqrt{\varepsilon_3}}\sec\theta_3, \quad (32)$$

$$\Delta\phi_4 = \frac{\omega}{c_0}\sqrt{\varepsilon_4}\,\Delta z_4 \cos\theta_4\,, \eta_4 = \frac{Z_0}{\sqrt{\varepsilon_4}}\sec\theta_4, \quad (33)$$

where c_0 is the free space speed of light. For identical lower and upper media, the reflectance R, transmittance T, and absorbance A can be calculated as follows [25]:

$$T = \tau\tau^*, R = \rho\rho^*, A = 1 - R - T, \quad (34)$$

where τ^* and ρ^* stand for the complex conjugate of the transmission and reflection coefficients, respectively.

3. Results and Discussion

In this section, we provide numerical examples of the propagation characteristics of the A-sandwich. For all numerical examples, the skin Glass epoxy (G) slab thicknesses are equal, i.e. $\Delta z_2 = d_1$, $\Delta z_4 = d_3 = d_1$, and the thickness of the core PU foam (F) slab is $\Delta z_3 = d_2$. The complex relative permittivity of the skin Glass epoxy slabs is $\varepsilon_2 = \varepsilon_4 = 4\,(1 - j0.015)$, while that of the core foam layer is $\varepsilon_3 = 1.15\,(1 - j0.002)$[23, 24]. Figures 2-4 illustrate the transmittance, reflectance, and absorbance of 3 GHz normally incident waves versus the ratio of core slab thickness to the free space wavelength λ_0. To investigate the effect of the G-layer thickness, calculations were performed for $d_1 = d_3$ within the range of 0.60-0.70 mm.

The curves of Fig. 2 show the transmittance at normal incidence versus the normalized core thickness d_2/λ_0 for different Glass epoxy slab thicknesses d_1. The theoretical transmittance curves presented in this work align perfectly with those obtained from COMSOL Multiphysics software for all parameters at normal incidence. All curves show that the A-sandwich structure under consideration is primarily transparent to electromagnetic waves in the S-band at all layer thicknesses under consideration, with a minimum transmittance of ~96%. In COMSOL simulation, the A-sandwich model is studied for one unit cell with applied Floquet boundary conditions that describe the periodicity. The Floquet periodicity can be used to model infinite periodic structures and models involving plane waves interacting with periodic structures [35, 36].

However, the transmittance exhibited a periodic behavior as d_2 increased, with a slight decrease in successive periods. The period of $0.466\lambda_0$ is precisely half the wavelength in the core medium with $\varepsilon_3 = 1.15$. Also, the reflectance exhibited similar periodic behavior with the same period as d_2 increases, and the reflectance minima coincide with the transmittance maxima (Fig. 3). The first transmittance maximum (with the highest transmittance of ~99%) occurs at $d_1 = 0.60$ mm and $d_2 \approx 3.0$ cm. The first transmittance maximum revealed an almost perfectly transparent structure with negligible reflection and only < 1% absorption as indicated by Figs. 2-4. The subsequent increase of d_2 by a multiple of half wavelength in the core material reproduced the transmittance maxima and reflection minima, as seen in Figs. 2 and 3. Evidently, the maximum values of the transmittance are almost independent of the value of d_1, which is a consequence of the vanishing effect of d_1 on the reflectance minima and the negligibly small increase of the absorbance with the increase of d_1, being ~ 0.1% across the whole range of d_1. However, the effect of d_1 on the minimum values of the transmittance is more pronounced owing to the more tangible increase of the maximum reflectance with the increase of d_1 leading to a reduction in the transmittance. Nevertheless, this reduction is still negligibly small for practical applications (< 1%). On the other hand, the small monotonic decrease (~ 1%) of the transmittance maximum value with the increase of d_2 from $0.3\lambda_0$ to $1.2\lambda_0$ is a result of the increase of absorption in progressively thicker layers of the core material.

Noteworthy, the periodic behavior of the transmittance in Fig. 2 and the reflectance in Fig. 3 are due to the dependence of K_3 from Eq. (29) on ϕ_3. The sine and cosine of $\Delta\phi_3$ vary with $d_2 = n\lambda$ and $d_2 = (n + 1/2)\lambda$ between +1 and -1, respectively, giving the periodic behavior of the transmittance and the reflectance as defined in Eq. (27).

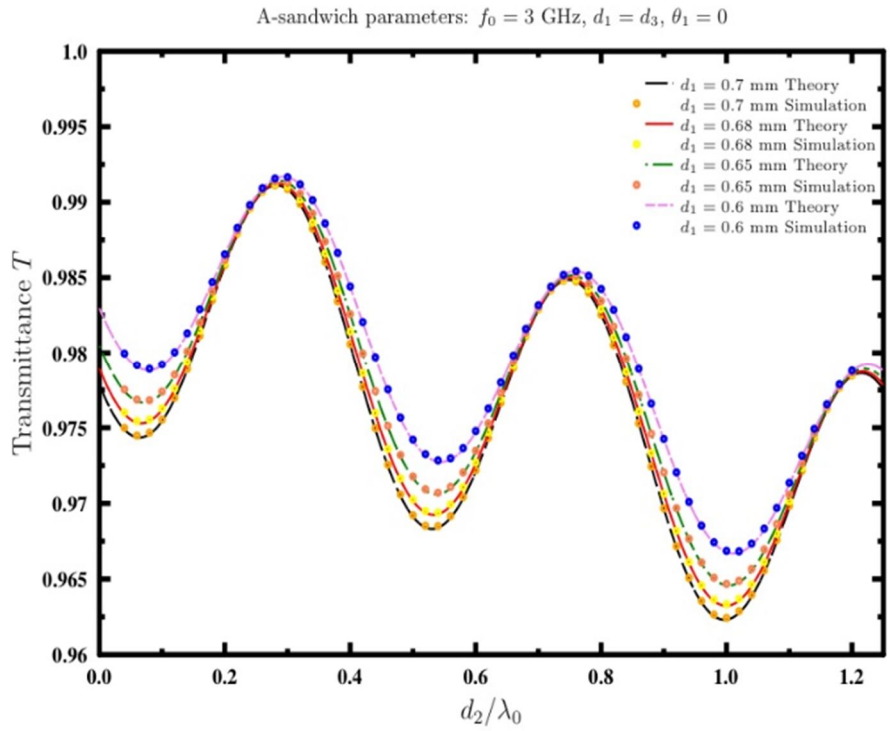

FIG. 2. Transmittance from theory and simulation for symmetric G-F-G unit cell.

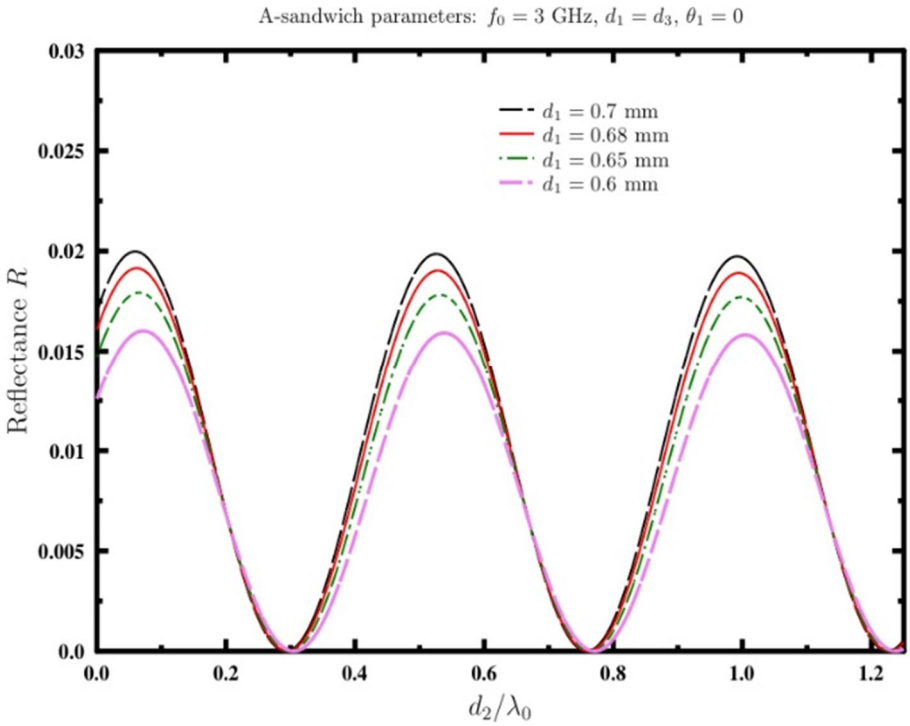

FIG. 3. Reflectance for symmetric G-F-G unit cell.

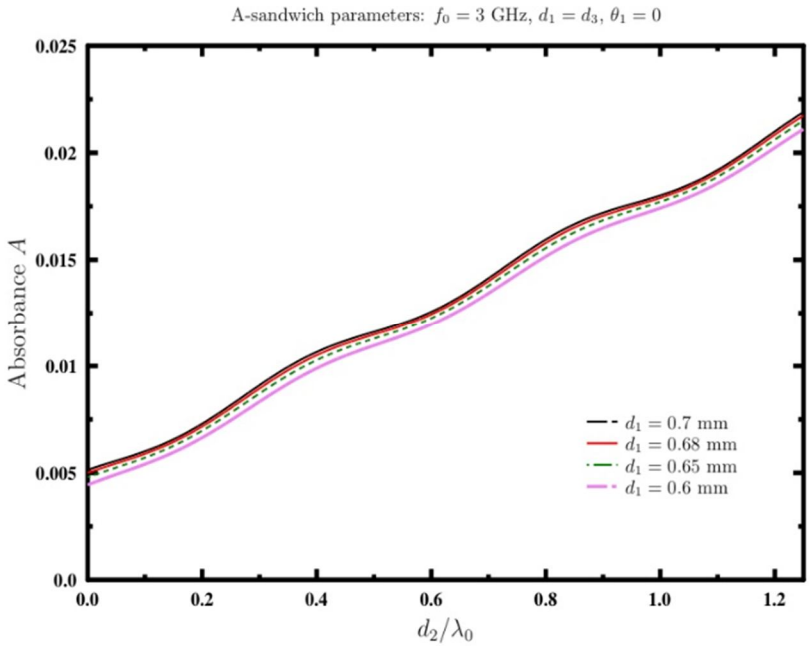

FIG. 4. Absorbance for symmetric G-F-G unit cell.

It is obvious from the above results that a skin thickness of d_1 = 0.60 mm provides better performance compared to larger values of d_1. Also, it is evident that the transmittance did not change appreciably with increasing core thickness d_2. However, the analysis of the propagation characteristics of the A-sandwich versus frequency in the range of 0-18 GHz, covering the S-band (2− 4 GHz) and the X-band (8 −12 GHz), reveals optimal performance at lower core thickness values. Figure 5 shows the frequency dependence of the transmittance at normal incidence for two A-sandwiches with d_1 = 0.60 mm, the first having d_2 = 0.5 cm and the second with d_2 = 3.0 cm. Obviously, at d_2 = 0.5 cm the A-sandwich maintains a high transmittance (above 95%) up to 14 GHz, beginning to degrade at frequencies higher than 12 GHz, reaching 77% at 18 GHz. In comparison, the transmittance of the A-sandwich with a core thickness of 3.0 cm exhibits oscillations in this frequency range, and a lower transmittance across the X-band and up to 15 GHz. The transmittance of this sandwich drops down to below 90% in the central region of the X-band, and down to 67% at 18 GHz. However, a slight improvement in performance is observed in a narrow frequency range of around 16 GHz.

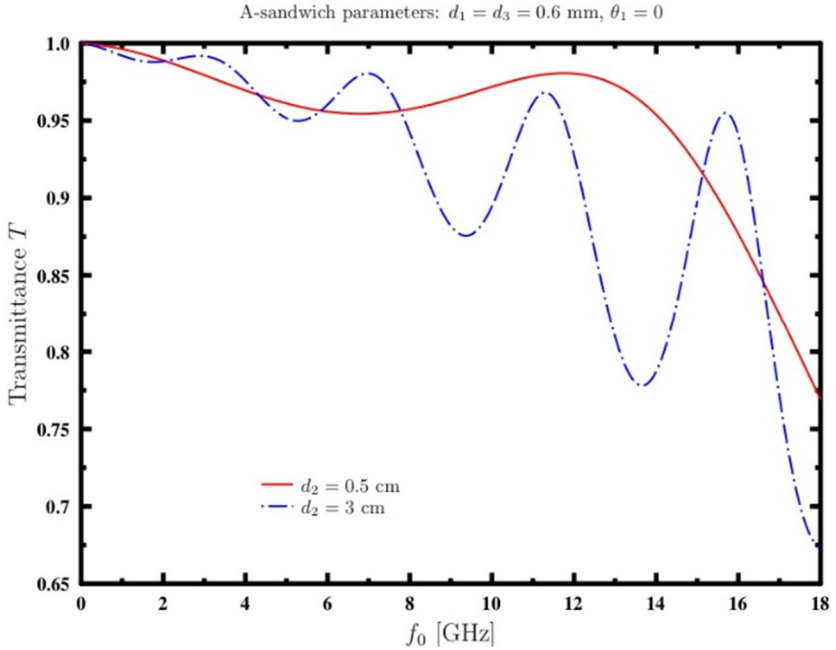

FIG. 5. Transmittance for symmetric G-F-G unit cell.

The fluctuations observed in Fig. 5 represent periodic oscillations in transmittance due to the dependence of $\Delta\phi_3$ on ωd_2. Accordingly, as the core thickness d_2 increases, the frequency range for a single oscillation period decreases. The superior performance of the A-sandwich with a core thickness of 0.5 cm is demonstrated by its low reflectance and absorbance across the X-band (Fig. 6). Conversely, the sharp increase in reflectance at higher frequencies is the primary factor responsible for the decline in transmittance for frequencies above 12 GHz.

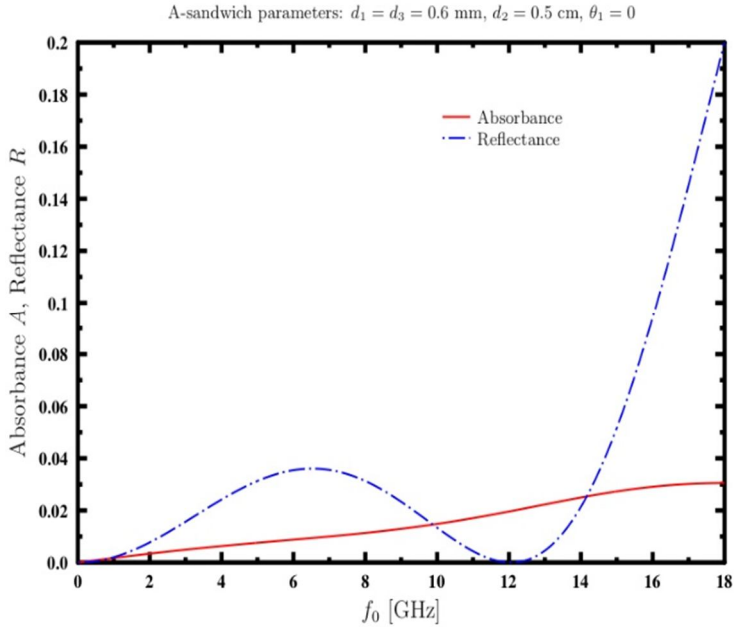

FIG. 6. Absorbance and reflectance for symmetric G-F-G unit cell.

To investigate the performance of the A-sandwich at arbitrary angles of incidence, the dependence of the transmittance on the angle of incidence was evaluated at the center of the S-band (3 GHz) and the center of the X-band (10 GHz) for the sandwiches with d_2 = 0.5 cm and d_2 = 3.0 cm. Figure 7 reveals high transmittance (> 92%) at 3 GHz for the sandwiches with d_2 = 0.5 and 3.0 cm up to an incident angle of 60°. At higher angles, the transmittance of both sandwiches drops rapidly to zero at grazing incidence, but the rate of decrease of the 3.0-cm sandwich is faster. At 10 GHz (Fig. 8), the 0.5-cm sandwich exhibits similar behavior, but with a faster decrease of transmittance with the increase of the angle of incidence, exhibiting 75% at 60°. However, the 3.0-cm sandwich exhibits a slow drop from 90% to a local minimum of 82% at 30° and subsequently increases to a maximum of 96% at ~ 52°, and then decreases rapidly to zero at grazing incidence. This sandwich exhibits higher transmittance than the 0.5 cm sandwich in the angular range of 45°-63°, but at higher angles, the transmittance dropps to zero at a faster rate. Accordingly, the sandwich with d_1 = 0.60 mm and d_2 = 0.5 cm can be suggested as a highly transparent radome wall for broadband electromagnetic waves at all angles of incidence. The behavior of the transmittance at the two different d_2 values in Figs. 7 and 8 is due to the dependence on $\Delta\phi_3$ which is proportional to $\omega d_2 \cos\theta_3$. As θ_3 increases above zero (normal incidence), the value of $\Delta\phi_3$ decreases leading to the observed behavior for d_2 = 3 cm.

Finally, we evaluated the transmission characteristics of the A-sandwich with d_1 = 0.60 mm and d_2 = 0.5 cm for perpendicular (TE) and parallel (TM) polarizations. At low angles of incidence, the sandwich revealed similar behaviors of the transmittance versus frequency with high transparency for both polarization modes in a broad frequency range (not shown for brevity). However, the frequency-dependent transmittance of the two modes showed different behaviors at higher angles of incidence. Figures 9 and 10 show representative curves of the transmittance versus frequency at an incident angle of 30°. Evidently, the A-sandwich revealed a high transparency (more than 90%) for both polarization modes up to 16 GHz, above which the transmittance starts decreasing rapidly. However, the transmittance of the TE mode was generally lower than the TM mode across the frequency range up to the end of the Ku band (18 GHz).

The average transmittance curves for both polarization modes at an angle of incidence $\theta_1 = \frac{\pi}{6}$ are shown in Fig. 10. By decomposing an incident wave into TE and TM wave modes, the average transmittance is obtained from $T_{av} = \frac{1}{2}(T_{TE} + T_{TM})$ [25]. Figure 10 shows that the theoretical results closely align with the simulation results, demonstrating almost identical transmittance values up to 18 GHz.

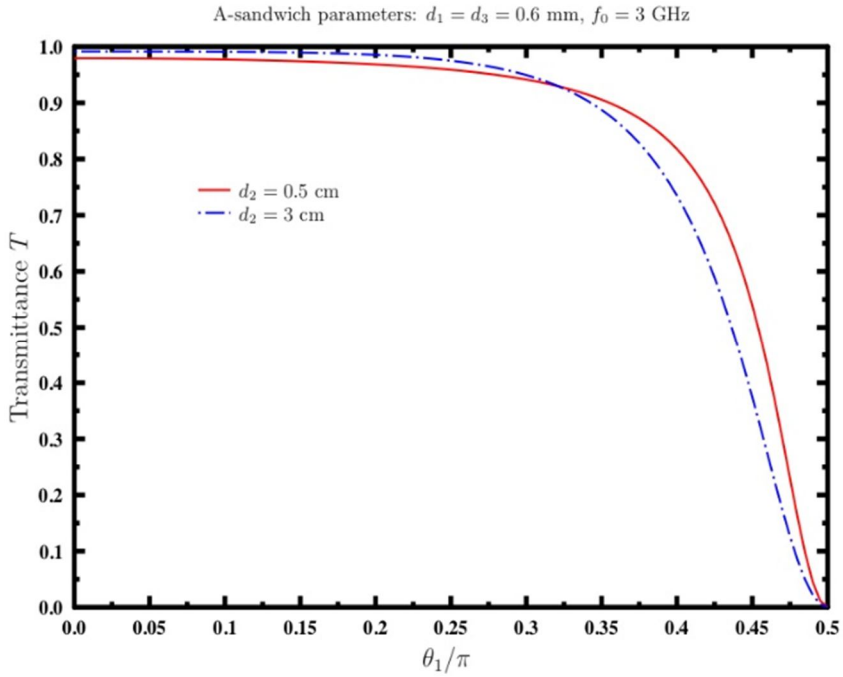

FIG. 7. Transmittance for symmetric G-F-G unit cell.

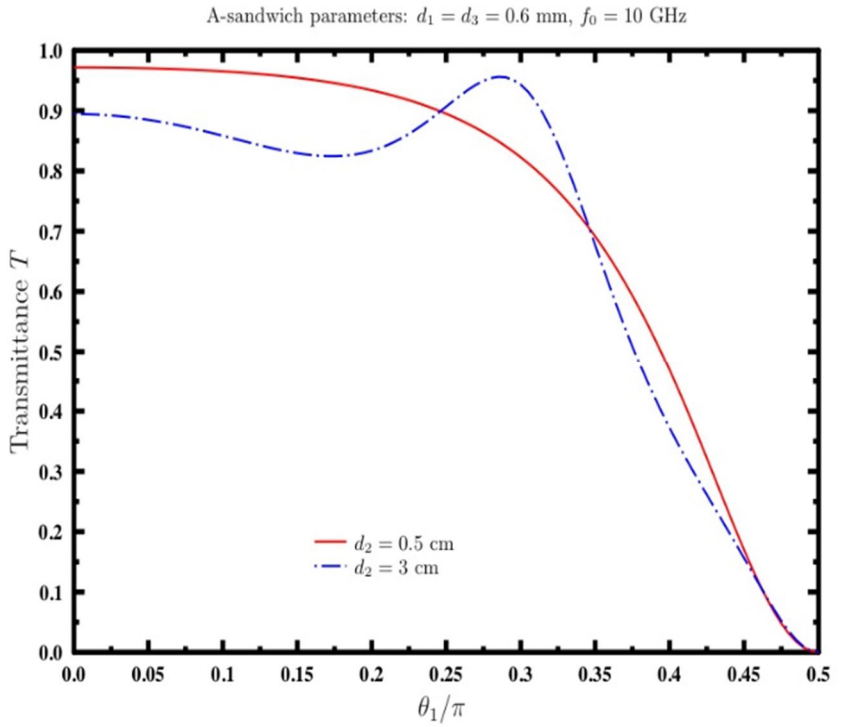

FIG. 8. Transmittance for symmetric G-F-G unit cell.

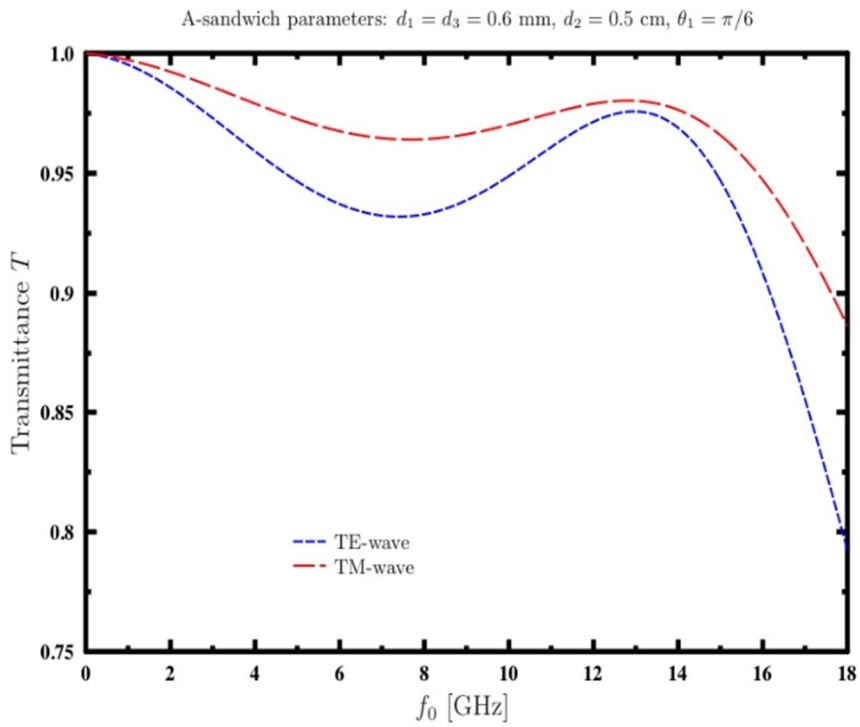

FIG. 9. Transmittance for symmetric G-F-G unit cell.

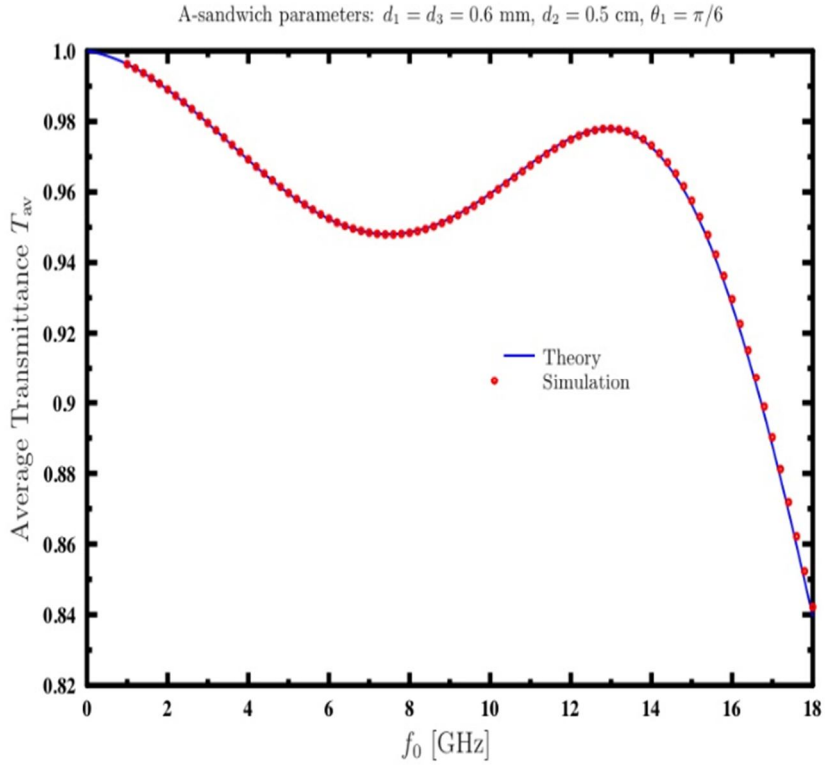

FIG. 10. Average transmittance from theory and simulation for symmetric G-F-G unit cell.

4. Conclusions

We investigated the propagation characteristics of the A-sandwich constructed from two identical skin Glass epoxy slabs and a core PU foam slab. The effects of slab thicknesses on transmission, reflection, and absorption behaviors were analyzed as the incident wave frequency and angle of incidence increased, utilizing representative numerical analyses derived from both theoretical models and simulations. The A-sandwich, with a skin layer thickness d_1 ranging from 0.60 to 0.70 mm and a core layer thickness d_2 of up to 12 cm, exhibited high transparency at 3 GHz normal

incidence conditions. However, the dependencies of the transmittance on the frequency and angle of incidence revealed a superior broadband performance of the A-sandwich with a lower core thickness compared to that with a higher core thickness, as demonstrated by the transmittance curves of the sandwiches with $d_1 = 0.60$ mm and core thicknesses of 0.5 and 3.0 cm. Generally speaking, the sandwich with a core thickness of 0.5 cm exhibited a high transparency, exceeding 95% at normal incidence across the frequency range from the S-band the X-band. Also, a high transmittance $\geq$ 92% at 3 GHz was observed for this sandwich at angles of incidence up to 60°. Even though the sandwich exhibited a small decrease of the transmittance at 10 GHz to the range of 98 – 82% at angles of incidence up to 55°, its performance is still of considerable practical importance. In addition, the A-sandwich exhibited a high performance for both TE and TM modes in a broad frequency range. These results from both theory and simulation indicate the feasibility of optimizing the A-sandwich radome wall for a broadband high performance in a wide range of angles of incidence. Further optimization of the skin and core layer thicknesses may provide only slight improvements in the A-sandwich transmission characteristics compared to the configuration we proposed for optimal performance. However, the mechanical strength of the radome wall constructed from the proposed A-sandwich should be investigated to ensure durability, robustness, and applicability for practical applications.

References

[1] Kozakoff, D. J., "Analysis of Radome-Enclosed Antennas", 2nd Ed., (Boston-London: Artech House, 2010).

[2] Cady, W., Karelitz, M. and Turner, L., "Radar Scanners and Radomes", MIT Radiation Laboratory Series Vol. 26, (McGraw-Hill, New York, 1948).

[3] Jones, D. S., "The Theory of Electromagnetism", (Pergamon Press Ltd., New York, 1964).

[4] Cornbleet, S., "Microwave Optics", (New York: Academic Press, 1976).

[5] Rudge, A. W., Milne, K., Olver, A. D., and Knight, P. "The Handbook of Antenna Design", Vol. 2, (Peter Peregrinus Ltd., London, UK, 1983).

[6] Shavit, R., "Radome Electromagnetic Theory and Design", 1st Ed., (John Wiley & Sons Ltd., 2018).

[7] Yurchenko, V. B., Altintas, A., and Nosich, A. I., IEEE Trans. Antennas Propag., 47 (1999) 668.

[8] Sunil, S., Venu, K. S., Vaitheeswaran, S. M., and Raveendranath, U., Microw. Opt. Techn. Lett., 30 (2001) 350.

[9] Nair, R. U. and Jha, R. M., Electron. Lett., 43 (15) (2007) 787.

[10] Nair, R. U., Neelam, A. and Jha, R. M., Appl. Electromagn. C. (AEMC), (2009), 1.

[11] Nair, R. U. and Jha, R. M, IEEE Trans. Antennas Propag., 57 (2009) 3664.

[12] Mei, Z., Xu, Y., Bai, J., and Cui, T., IEEE Trans. Opt. Express, 20 (2012) 16955.

[13] Sunil, C., Daniel, A., Rao, B. S., Kumar, V. S. and Sarkar, M., IEEE Indian C. Antenn. Propag. (InCAP) - Hyderabad, India (2018) 16.

[14] Nair, R. U., Shashidhara, S. and Jha, R. M., IEEE Antenn. Wirel. Propag. Lett., 11 (2012) 854.

[15] Lee, K., Chung, Y., Hong, I. and Yook, J., IEEE Antennas and Propagation Society International Symposium, (2010), pp.1-4.

[16] Duxian, W., J. Electron., 11 (4) (1994) 332.

[17] Lee, K. W., Chung, Y. C., Hong, I. P. et al., IEEE Antennas and Propagation Society Int. Symp. (APSURSI), Toronto, Canada, (2010), pp. 1-4.

[18] Walton, J. D., "Radome Engineering Handbook: Design and Principles", Vol. 1, (New York: M. Dekker, 1970).

[19] Choi, I., Kim, J. G., Lee, D. G., and Seo, I. S., Compos. Sci. Technol., 71 (14) (2011) 1632.

[20] Nazari, F., Taherkhani, M., Mokhtari, M., Aliakbarian, H., and Shekoofa, O., IET Sci. Meas. Technol., 14 (2020) 808.

[21] Zhou, L., Pei, Y. and Fang, D., IEEE Antenn. Wirel. Pr., 15 (2015) 218.

[22] Jasik, H., “Antenna Engineering Handbook”, (McGraw-Hill, New York, 1961).

[23] Mahima, P., Suprava, M., Vandana, S., Yazeen, M. P. S., and Nair, R. U., "Electromagnetic Performance Analysis of Graded Dielectric Inhomogeneous Radomes", (Springer Briefs in Applied Sciences and Technology, Springer, Singapore, 2018).

[24] Yazeen, P. S. M., Vinisha, C. V., Vandana, S., Suprava, M., and Nair, R. U., "Broadbanding Techniques for Radomes", (Springer Briefs in Electrical and Computer Engineering, Springer Nature Singapore Pte Ltd. 2020).

[25] Pedrotti, F. L., Pedrotti, L. M., and Pedrotti, L.S., "Introduction to Optics", 3rd Ed., (Cambridge University Press, 2017).

[26] Pozar, D. M., "Microwave Engineering", 4th Ed., (John Wiley & Sons, New York, 2012).

[27] Dobrowolski, J. A., "Microwave Network Design Using the Scattering Matrix", (Artech House, Boston/London 2010).

[28] Benson, F. A. and Benson, T. M., "Fields, Waves and Transmission Lines", 1st Ed., (Springer-Science, Business Media, B. V. 1991).

[29] COMSOL, "COMSOL Multiphysics 4.3 Users Guide", (2012).

[30] De Vita, F., Di Marco, S., Costa, F., and Turchi, P., "Design of a Stealthy Antenna Using COMSOL Multiphysics", (Excerpt from the Proceedings of the 2012 COMSOL Conference in Milan).

[31] Cross, L. W. and Almalkawi, M. J., "Scan Angle Stability of a Second-Order Plasma-Switched Frequency Selective Surface", (Excerpt from the Proceedings of the 2013 COMSOL Conference in Boston).

[32] Lu, Y., Chen, J., Li, J., and Xu, W., Materials, 15(2) (2022) 640.

[33] Ali, N. M. and Ali, T. A., Appl. Phys. B, 129 (2023) 15.

[34] Cai, F. and Ko, Z., Photonics, 10 (2023) 643.

[35] Guillod, T., Kehl, F., and Hafner, C., Prog. Electromagn. Res., 137 (2013) 565.

[36] Alaverdyan, S. A., Kabanov, I. N., Komarov, V. V., and Meschanov, V.P., IEEE T. Microw. Theory, 63 (8) (2015) 2509.